Prototype NOvA RF Cavity for the Fermilab Recycler Ring

Heba Elnaiem

Fermi National Accelerator Laboratory

&

Howard University

May 18th – August 7th 2009

Abstract

As part of the NOvA project the Fermilab Recycler Ring will be converted to a pre-injector to the Main Injector. This upgrade allows the cycle time to be reduced from 2 seconds to 1.33 seconds; thus yielding an increase in beam power, which can be accredited to two slip stacking cavities in the Recycler Ring. Therefore in this study we built an inexpensive, low power prototype of this NOvA RF cavity. The prototype RF cavity, proved to be useful in identifying various higher order modes, as well as in measuring key parameters associated with the main mode such as Q, dependence of frequency on gap spacing, and sensitivity to tuner depth and z position.

Introduction

Little is known about the elusive particles known as neutrinos, beyond their angular momentum, and the fact that they oscillate and have a mass. The difficulty in the research of these particles lies in the fact that neutrinos interact very weakly and are therefore difficult to detect. We now believe neutrinos oscillate between different flavors, but the questions are how do they do so and what are the timescales of oscillations? [1]. At Fermi National Accelerator Laboratory scientists use accelerators to create intense beams of trillions of particles for neutrino experiments and measurements of this ultra-rare process. Fermilab is a leading Department of Energy research lab that is dedicated to understanding the fundamental nature of matter and energy.

The "Neutrinos from the Main Injector" (NuMI) beamline is a facility at Fermilab which uses protons from the Main Injector accelerator to produce an intense beam of neutrinos [2]. The NOvA (NuMI Off-Axis Electron Neutrino Appearance) experiment will use the existing NuMI beam to search for evidence of muon to electron neutrino oscillations. This oscillation, if it occurs, will hold the key to many of the unanswered questions in neutrino physics; such as the ordering of the neutrino mass states. The NOvA detector will be located slightly off the centerline of the neutrino beam. This off-axis location produces a large neutrino flux that peaks at 2 GeV, the energy where oscillations to electron neutrinos is expected to be a maximum. As part of the NOvA project, the accelerator infrastructure and the NuMI beam line will be upgraded to provide higher neutrino intensities than are currently possible in the NuMI beam. With the conclusion of the Tevatron collider program at Fermilab, the Recycler ring, which is currently used to store anti-protons, can be converted to a pre-injector to the Main Injector. This allows the cycle time to be reduced from 2 seconds to 1.33 seconds, yielding an increase in beam power [3].

An upgrade goal for the NuMI beam line is to double its intensity by accelerating 6 Booster batches in the Main Injector with twice as many protons per batch, which is possible via slip-stacking. Two RF cavities with different frequencies are used for the 12-batch slip stacking. Six batches are injected on the central frequency of the first RF system, 52.814MHz, and captured with 110kV RF voltage, then decelerated. The second RF cavity is off during the first 6 batch injections. After the frequency of the first cavity is lowered, the 7^{th} batch is injected on the central frequency of the second RF system and captured with 110kV RF voltage, then accelerated. Since the 7^{th} injection batch and the other six have different frequencies and energies, they move on different orbits in the ring and do not interact. After the batch train slips by about one batch length, the 8^{th} batch is injected on the central frequency, captured by the second RF cavity and accelerated. Then this same process that occurred for the 8^{th} batch is repeated for batches 9-12. After the 12th batch is injected, both frequencies are changed to the central frequency at which time both the higher and lower energy batches stack upon each other longitudinally [4]. When the bunches are aligned, the beam is extracted from the recycler and injected into the Main Injector (MI) where they are captured in RF buckets corresponding to a 2MV RF voltage. Therefore, during the next turn, the Main Injector will accelerate 6 Booster batches that have twice as many protons. Thus creating a more efficient accelerator, because the

cycle in the MI is decreased from 2 seconds to 1.33 seconds since slip stacking is performed in the recycler ring.

The upgrade of the recycler ring requires a new RF cavity to be installed for the new NovA experiment. This investigation describes the building of a low power, inexpensive model RF cavity as a prototype for the actual high power RF cavity, which will be installed in the Fermilab Recycler Ring. The objective of our study was to build and study as many factors about the cavity as possible before the $2 million NOvA cavities are installed to the Recycler Ring.

Materials and Method:

Cavity Dimensions:

The cavity, illustrated in figure 1, is a coaxial quarter wave resonator which is open on one end and shorted on the other end. The calculation of both the outer and inner radii was dependent upon the power available and the desired center frequency, R_{sh}/Q and voltage across the gap (150kV). The maximum power that would be available to this RF cavity once it was installed is 150kW. This power factor along with the desired gap voltage determines the R_{sh} as seen in equation 1 as 75000Ω. An important factor that sets this cavity apart from similar cavities is its low R_{sh}/Q which is only 14Ω; therefore the Q value is dictated to be 5000. A low Rsh/Q is desired in order to reduce beam loading effects. Furthermore, this cavity will have a center frequency of 52.814MHz, so r_1 and r_2 can also be calculated from equation 2 with the consideration that the $r_2 \leq 17$ inches. Since this cavity is to be installed to the Recycler Ring, which hangs from the ceiling of the same tunnel that harbors the main injector, its dimensions need to fit in this pre-designated area which requires $r_2 \leq 17$ inches. Thus, equation 2, in which σ is the conductivity of copper, determines r_1 to be 13.38 inches and r_2 16.07 inches.

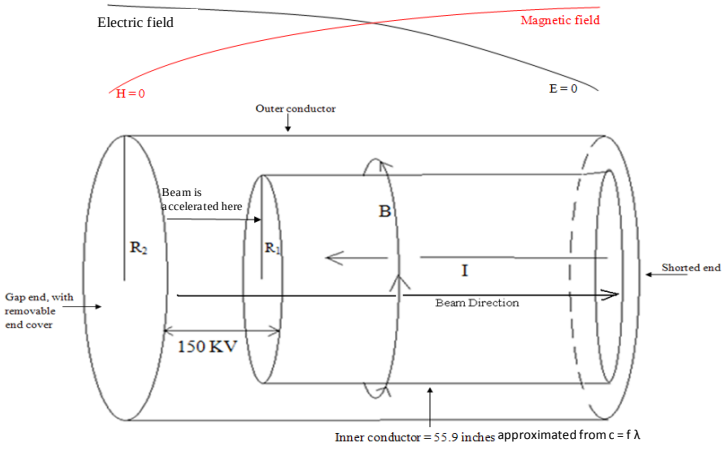

Figure 1: A schematic of the cavity diagramming r_1, r_2, the desired gap voltage, the beam, the current and the B directions of propagation. Also, the value of the magnetic field (B) and electric field (E) are shown as sin/cos dependent.

$$R_{sh} = \frac{(V_{gap})^2}{2P} \qquad (1)$$

$$Q = \frac{\omega L}{R} = \frac{2\,(\pi\mu_o\sigma f)^{1/2}}{1+(r_2/r_1)}\, r_1 \ln\frac{r_2}{r_1} \qquad (2)$$

With the values of r_1 and r_2 determined it is important to consider and account for the phenomena of multipactoring. Electron multiplication by secondary emission can occur when an oscillating potential is applied between two surfaces in a vacuum and if the voltage, frequency,

and spacing are such that the time of flight of an electron between the surfaces is an odd multiple of a half period of oscillation [5]. When this occurs in a cavity it may produce a heavy load which will decrease the cavity voltage. However, the conditions of multipactoring can easily be derived to ensure that it does not occur in this cavity. The threshold voltage at which multipactoring occurs is easily calculated from equation 3 where f is the frequency in MHz and d is the spacing in inches:

$$V_t = 0.039(fd)^2 \quad (3)$$

As long as the threshold voltage is less than the desired voltage across the gap then this phenomena does not occur. In this study it is not a problem because the threshold voltage is only 679.9V which is not comparable to the 150KV desired across the gap. It is important to note that the voltage throughout the cavity is expressed as Sin(d), where d is the distance from the shorted end. The voltage is at a maximum of 150KV at the end of the inner conductor because this is a $\lambda/4$ resonator, and then it is constant across the gap.

Cavity Design

After calculating both the inner and outer conductor radii, the assembly design was selected. Since this will be a $\lambda/4$ resonator, the total cavity length can be calculated using the electromagnetic wave frequency equation.

$$c = f\lambda \quad (4)$$

Thus the length of the inner cavity must be 55.91 inches, because the center frequency is 52.814 MHz. The length of the outer conductor is 60 inches, because a gap cover will be placed on it; therefore the gap distance can be adjusted to the desired spacing. The circumference of each conductor is calculated to be $2\pi r$, therefore the inner conductor is 84.8 inches and the outer is 100.5 inches. Since there were only six 3ft x 8ft rectangular copper sheets available, each conductor was made from several sheets that were bolted together with overlapping areas of 2 inches, as seen in figure 1.

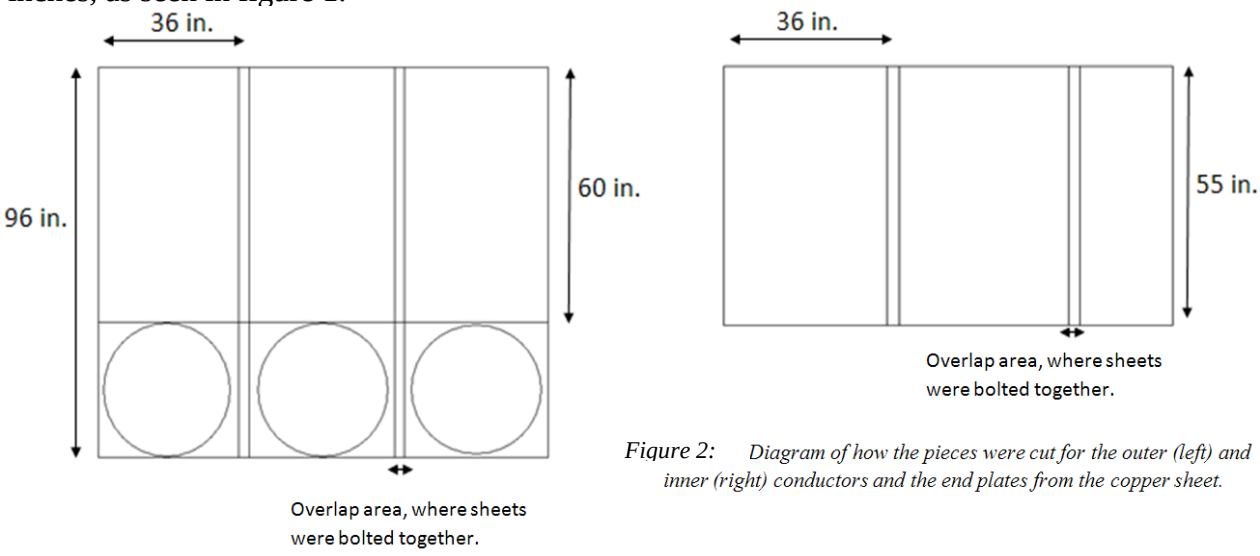

Figure 2: Diagram of how the pieces were cut for the outer (left) and inner (right) conductors and the end plates from the copper sheet.

After the sheets were secured into rectangles of the appropriate dimensions, both the inner and outer conductors were formed into cylinders that are 55 inches and 60 inches high. The cylinderical inner conductor is seen in figure 3. Then from the remaining sheets of copper the

end covers were created, as seen in figure 2. Two end plates were cut to fit the circumference of the outer conductor, and one was cut to fit that of the inner conductor, as seen in figure 4 (left). One of the end plates that is to fit the outer conductor was cut in the center to include a hole for the inner conductor so it fits in the shorted end of the cavity.

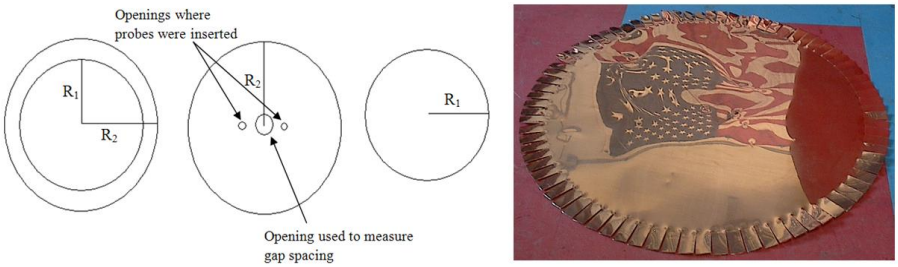

Figure 4: To the left is a diagram of the cavity endplates, and to the right is an endplate without the fork bent at 90°. These forks act like springs and make good electrical contact.

Figure 3: Inner conductor after it has been formed into a cylinder.

Furthermore, forks were created in each of the end plates because they act like springs and make good electrical contact, as seen in figure 4 (right). Moreover figure 5 is a picture of the cavity after full assembly.

Figure 5: Prototype cavity after assembly with a polystyrene board for support.

Theory

This new NOvA cavity is different from many previous ones, because of its low R_{sh}/Q. The Rsh/Q of this cavity is only 14Ω as compared to that of the main ring which currently has an R_{sh}/Q value of 106Ω. While having a low R_{sh}/Q requires much more power, this is beneficial because it is less susceptible to transient beam loading effects. Transient beam loading causes the voltage to drop, which requires more power which is why it is essential that it does not occur.

This low R_{sh}/Q value is created through a series of resultant factors. The low requirement of a beam induced voltage across the gap dictates a large capacitance, resulting in a lower impedance line thus making R_{sh}/Q small. Therefore, it is important to keep the capacitance across the gap as large as possible to maintain the desired values of both the frequency and R_{sh}/Q. The capacitance across the gap causes the frequency to be lower than what one would calculate given that the center conductor has a length of $\lambda/4$, equation 6 allows one to solve for the corrected frequency. The gap capacitance of the cavity is calculated from equation 6 to be 58.8 pF, where $\beta = 2\pi / \lambda$, Rc is the characteristic impedance described in equation 5, and Lr is length of inner conductor.

$$\mathrm{Tan}\,(\beta L_r) = \frac{1}{\omega R_c C_{gap}} \tag{5}$$

$$R_c = \frac{1}{2\pi}\left(\frac{\mu_o}{\varepsilon_o}\right)^{1/2} \ln\left(\frac{r_2}{r_1}\right) = \frac{\pi R_{sh}}{4\ Q} \tag{6}$$

The fact that R_0/Q_0 is independent of losses makes it possible to conduct laboratory measurements without regard to their presence (note that the subscripts denote the values of R and Q at resonance). Since R_0/Q_0 is proportional to the frequency, it can be determined by measuring the rate of change of frequency with changes in capacity. The value of R_0/Q_0 is simply a geometrical factor that can be found by perturbation techniques; which involve the measurement of the resonant frequency of the cavity as a function of position of certain perturbing objects.

According to Maier and Slater, if some object is introduced into a cavity in a region where the magnetic field is essentially zero, the resonant frequency will change because the altered fields correspond to a change in capacity in the low-frequency case. Thus, the presence of the perturbing object increases the capacity and lowers the frequency. Therefore, it is necessary to relate the change in frequency of a microwave cavity to the volume, shape, material, and position of the perturbing object [6]. The relationship is obtained from the Slater perturbation theorem

$$\omega^2 = \omega_o^2\left(1 + k\frac{\int_{\Delta\tau}(\mu H^2 - \varepsilon E^2)\,d\tau}{\int_V(\mu H^2 + \varepsilon E^2)dv}\right) \tag{7}$$

where $d\tau$ is an element of the volume of the perturbing object and dv an element of volume in the cavity. In our case since the perturbation is small, $\omega = \omega_o$, $\delta = (\omega - \omega_o) / \omega_o$, and

$$\delta = \frac{\kappa \int_{\Delta\tau}(\mu H^2 - \varepsilon E^2)\,d\tau}{4U} \tag{8}$$

where U is the stored energy, E is the electrical field and H is the magnetic field which is equal to $H = B/\mu$. This important relation states that the perturbed frequency ω is changed from the natural resonant frequency ω_o by an amount which depends upon the integral $\int_{\Delta\tau}(\mu H^2 - \varepsilon E^2)\,d\tau$ over the volume removed by the perturbing object $\Delta\tau$ [6].

The Q of the structure depends upon its physical dimensions, the material used, and the operating frequency [7]. Q is defined as

$$Q = \frac{(2\pi)\,(\text{Stored Energy})}{\text{Energy Dissipated per Cycle}} = \frac{2\pi f\, W_{st}}{\text{Power loss}} = \frac{f}{\Delta f} \qquad (9)$$

where f is the actual frequency and Δ f is the bandwidth. As seen in equation 9 the Q value also depends upon the frequency being tested, which is why in our cavity we observed a large range of Q values at different modes. This is also consistent with the equation because there are different energies stored in various parts of the cavity and different power losses. This variation of Q value for different modes is shown in Appendix table 1. However, the Q value of 5357 is that of the center frequency, 52.814MHz.

Results and Discussion

The gap distance, which is the spacing between the inner conductor and the cavity endplate on the open end, can be adjusted by moving the endplate away from the inner conductor. Thus, we measured the relationship between the gap distance and center resonant frequency of 52.814MHz. By changing the gap distance we are essentially changing the capacitance, and therefore modulating the frequency as seen in equation 5. This relationship can be seen in figure 7 which is a plot of the distance between the inner cavity and the gap endplate vs. the frequency, this data is available in Appendix table 2. The plot below illustrates that the greater the gap spacing the larger the frequency.

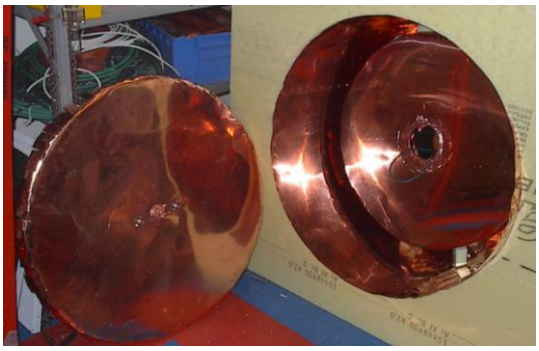

Figure 6: Gap with the end plate taken off.

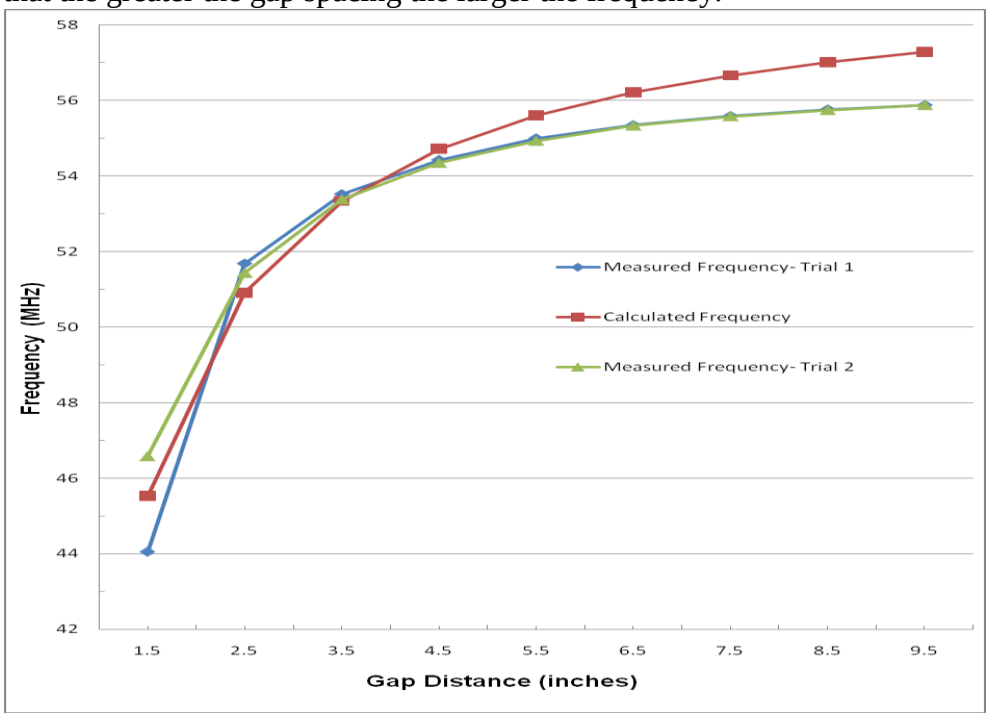

Figure 7: Measurements of Frequency with respect to gap distance. Note that trials 1 and 2 were performed under the same conditions and overlap starting at 3.5 inches. Also, the calculated frequency is based on equation 5.

No cavity will always resonate at the exact same center frequency. There are various reasons for this, including environmental factors such as temperature. Since the temperature in the recycler ring tunnel is not kept constant, a tuner is required to set the frequency precisely. Accounting for this factor three holes were cut in the middle and either end of the cavity. An aluminum tuner of diameter 3.2 inches and a height of 2 inches, shown in figure 8, was inserted into each of these holes. Figure 9 illustrates how the frequency is changed by this tuner in different ways when placed in the various holes. During the insertion its depth into the cavity was measured by tenth of an inch markings on the tuner itself.

Figure 8: aluminum cavity tuner with dia. of 3.2 inches used to tune the frequency of the cavity.

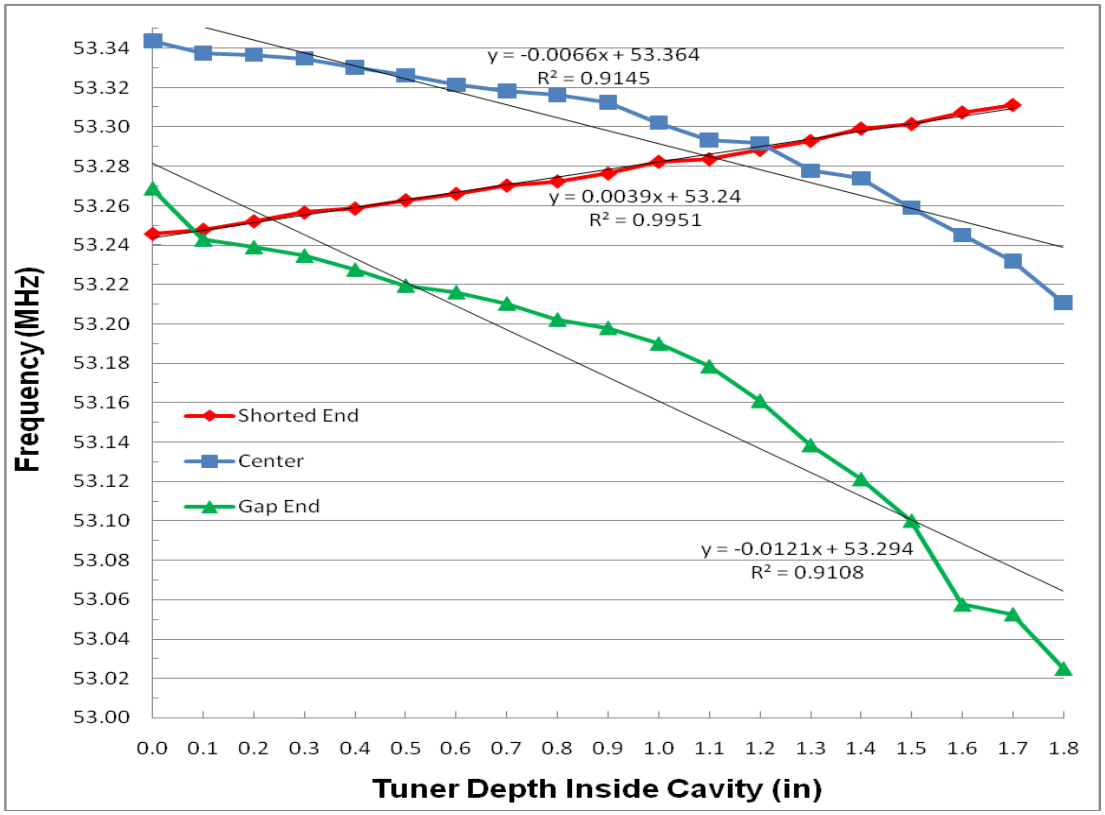

Figure 9: Frequency at a constant gap distance (3.5") with respect to tuner length measured with tuner in different ends of the cavity. This data is available in Appendix table 3.

Figure 10: aluminum sphere with dia. of 0.8 inches used to tune the frequency of the

Notice that the center frequency decreases with respect to the tuner depth for both the Center and Gap end, and increases in the Shorted end. This relationship agrees with the Slater perturbation equation because in the Shorted end the electrical field is essentially zero which is why the frequency increases with tuner depth. The inverse is true for the Gap end, where the magnetic field is zero. In the Center both the electrical field and the magnetic field should be equal. The changes in frequency observed with this tuner are too large to make delicate adjustments to the frequency, which is what is needed when this cavity will be installed. Therefore, a small aluminum sphere tuner of diameter 0.8 inches was used instead. By using this sphere tuner, shown in figure 10, the Slater perturbation method for metallic spheres can be applied. As seen in table 1, this small cylinder makes delicate adjustments to the frequency of the cavity which is required. As seen in table 1 the sign of the change in frequency is consistent to the predicted values. Furthermore, the calculations of the measured change in frequency compared to that of the calculated are very close. Therefore, this is a more accurate and precise method of adjustment to the frequency.

Table 1: Slater perturbation method with small cylinder

	Shorted End	Center End	Gap End
δ f measured	2180.00 Hz	-1600 Hz	-4900 Hz
δ f calculated	1764.99 Hz	-1667 Hz	-3250.4 Hz

TEM harmonic modes

In this quarter-wave coaxial resonator two classifications of modes are present: TEM (transverse electromagnetic) modes and H_{m1} ring modes. The TEM modes are the λ/4 modes that propagate down the cavity, which acts like a coaxial wave guide. The TEM mode of concern is the center frequency, of 52.814MHz which is used to accelerate/decelerate the beam during slip stacking. However, there are higher order odd harmonic TEM modes which are unavoidable, these modes can be seen in figure 11.

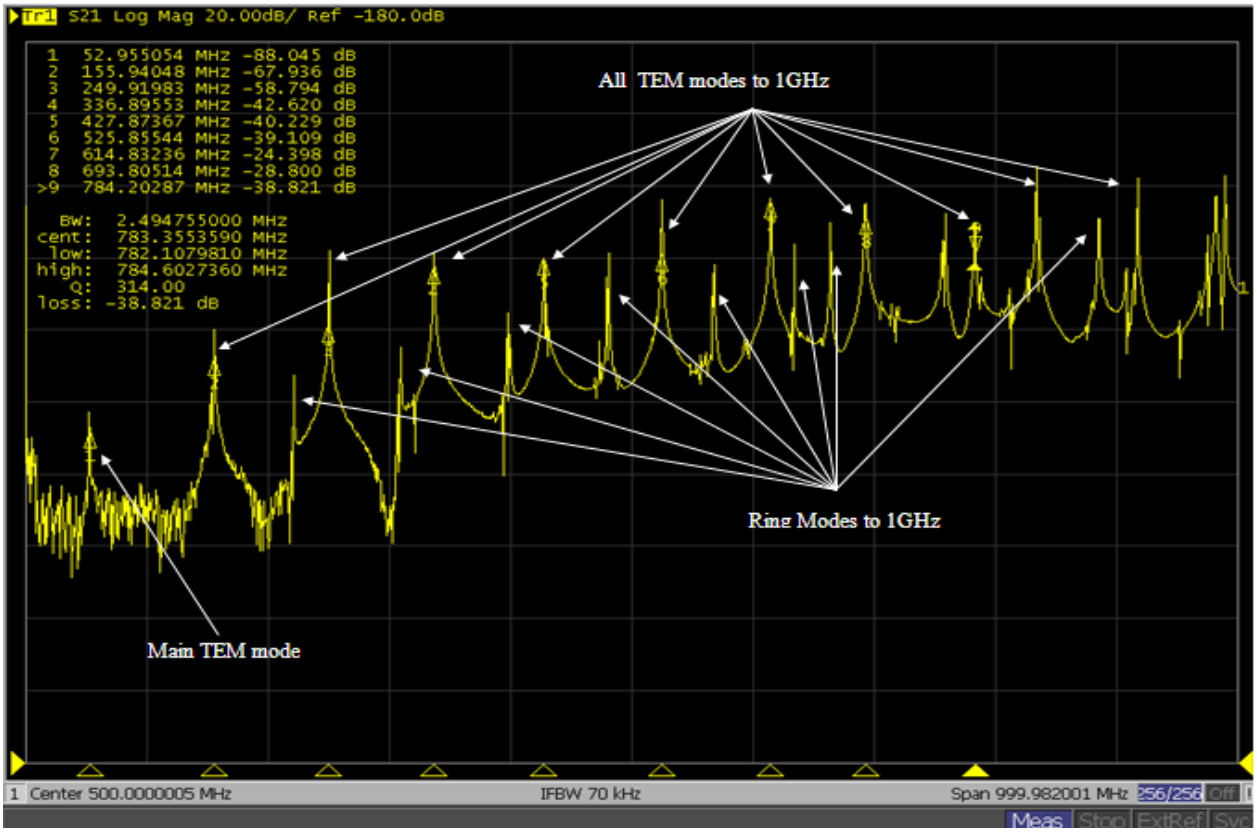

Figure 11: Network Analyzer data measurement of all TEM modes found up to 1GHz, with the markers on individual TEM modes. The main TEM mode appears to be smaller than the other TEM modes because its resonance is so narrow that there are not enough points on this network analyzer image to view its actual amplitude. Furthermore, the pickup is more sensitive to higher frequencies so the higher order TEM modes appear to have larger amplitudes.

Therefore, it is important to measure all modes in order to damp unwanted ones during slip stacking. This quarter-wave TEM resonator is slightly foreshortened by a capacitance at the high voltage end. The odd higher order harmonic modes do not simply stop at the end of the inner conductor but propagate into the gap spacing, which forms a radial waveguide. These higher order TEM modes do not fully fit the length of the inner conductor, so the remaining section of the wave propagates into the radial waveguide. In fact the magnetic and electric fields of both the coaxial and radial waveguides couple strongly, which is another factor that results in the radial movement of these modes into the center of the gap spacing. The radial waveguide has a cutoff wavelength expressed by equation 10, where r_1 is the radius of the inner conductor in meters. Therefore the cutoff wavelength of the radial waveguide is 139MHz.

$$\lambda_{cutoff} = \frac{2\pi r_1}{c} \tag{10}$$

The measured modes seen in figure 11 were then identified to their corresponding calculated harmonic mode. The calculated harmonic higher order modes are simply the harmonic number times f_o.

Table 2: Classification of all higher order harmonic TEM modes

Measured modes	Calculated modes	Type of TEM mode
52.65743	52.814	Main
156.03394	158.442	3rd harmonic
250.63153	264.07	5th harmonic
337.42565	369.698	7th harmonic
428.41776	475.326	9th harmonic
525.81614	580.954	11th harmonic

Ring Modes

Ring modes are the other classification of modes found in this quarter-wave coaxial resonator. There are different types of Ring modes including E_{mn}, H_{mn} and H_{m1}. The type that affects this cavity are H_{m1} modes. The cutoff wavelengths of both E_{mn} and H_{mn} ring modes has an (a-b) dependence, as seen in equation 11 and 12 respectively, where a is the diameter of the outer conductor and b is that of the inner conductor in inches.

$$E_{mn}\,\lambda_{cutoff} = \frac{2(a - b)}{n} \tag{11}$$

$$H_{mn}\,\lambda_{cutoff} = \frac{2(a - b)}{(n - 1)} \tag{12}$$

Since both equations have an (a-b) factor, which causes a small λ, the cutoff frequency is very large and is not observed in the 1 GHz range. For example, if n = 1 the E_{m1} cutoff frequency is 2.36GHz and if n=2 the H_{m2} cutoff frequency is also 2.36 GHz. However we are focusing on only the H_{m1} because they have cutoffs that are closer to the higher order harmonic TEM modes, due to their (a + b) dependence.

$$H_{m1}\,\lambda_{cutoff} = \frac{\pi\,(a + b)}{m} \tag{13}$$

The predicted wavelengths of the ring modes are calculated as

$$\lambda = \frac{\lambda_g}{\left(1 + \left[\lambda_g / \lambda_{cutoff}\right]^2\right)^{1/2}} \tag{14}$$

where λ_{cutoff} is that of the H_{m1} modes, and λ_g is the guide wavelength which is defined as

$$\text{Length of the inner conductor} = \frac{n\,\lambda_g}{4}$$

$$n = 1, 3, 5, 7\ldots \tag{15}$$

These calculated wavelengths are used to identify the measured modes not only with respect to their m values, but also individual $n\lambda_g$ as seen in Table 3.

Table 3: Classification of measured ring modes up to 520MHz, with respect to their λ_g as well as color codes due to their m values

Measured modes	Calculated modes	Type of Ring mode
149.29344		
153.63287	141.0	$\lambda_g/4$, m=1
218.81737		
221.61862	221.0	$3\lambda_g/4$, m=1
274.04195	261.9	$\lambda_g/4$, m=2
306.81203		
310.01315	312.5	$3\lambda_g/4$, m=2
316.27794		
321.21844	327.1	$5\lambda_g/4$, m=1
387.04774		
391.44970	387.0	$\lambda_g/4$, m=3
393.85077		
397.45237	394.7	$5\lambda_g/4$, m=2
399.99100	422.9	$3\lambda_g/4$, m=3
430.21889	422.9	$3\lambda_g/4$, m=3
430.81926		
470.84428	440.7	$7\lambda_g/4$, m=1
474.04628		
479.44966	486.8	$5\lambda_g/4$, m=3
482.85178		
487.25453	492.8	$7\lambda_g/4$, m=2
517.61101		
520.01251	513.3	$\lambda_g/4$, m=4

Ring modes have varying magnetic and electric field distribution in the phi and r directions, which are proportional to and dependent upon sin/cos (mΦ). Also the magnetic field has an additional component in the z direction. Figure 13 is a visual representation of the field distribution for H_{m1} for m = 1, 2, and 3.

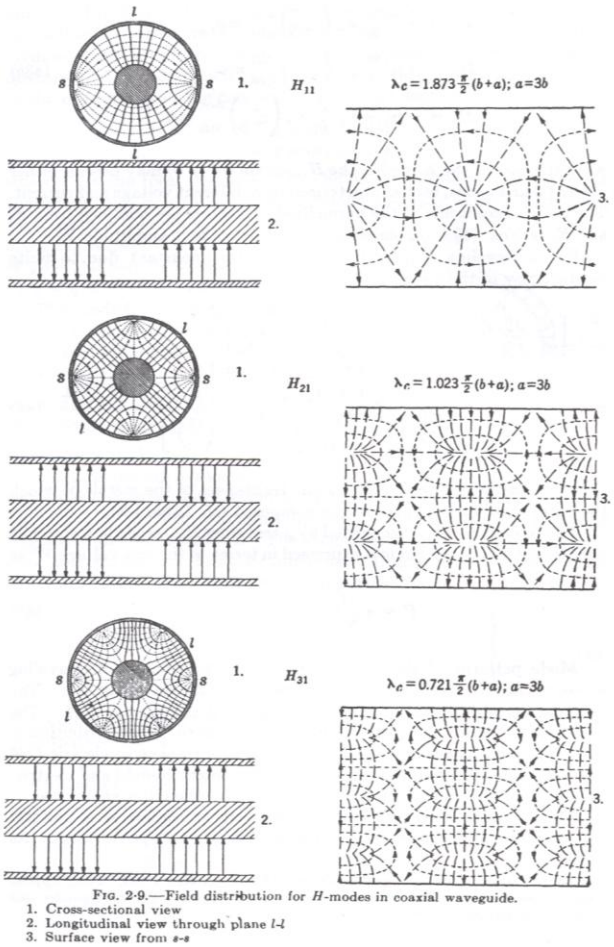

FIG. 2-9.—Field distribution for H-modes in coaxial waveguide.
1. Cross-sectional view
2. Longitudinal view through plane l-l
3. Surface view from s-s

Figure 13: Diagram illustrates the field distribution for H_{m1} for m = 1, 2, and 3.

Since TEM modes have no component in the z direction, whereas ring modes do, the two can be distinguished by observing fluctuations in amplitude when changing the orientation of the loops of the pickup.

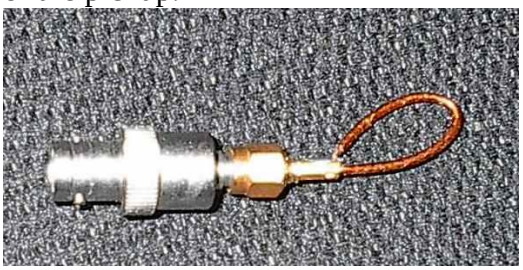

Figure 14: Power coupler pickup loops, used to measure the modes in the cavity.

Conclusion

The prototype RF cavity built in this study, proved to be useful in identifying various higher order modes, as well as in measuring key parameters associated with the main mode such as Q, dependence of frequency on gap spacing, and sensitivity to tuner depth and z position. While the measurements preformed in this study gave a general overview of what is to be expected in the NOvA cavity, it is still useful to perform further measurements. Currently work is being performed to study factors including measurement of the Rsh, damping of the higher order modes and quantifying the effect of the power coupler.

Acknowledgements

This research was conducted at Fermi National Accelerator Laboratory. I thank Dianne Engram, Jamieson Olsen and the rest of the SIST committee for the opportunity to participate in this program. In particular, I would like to thank my supervisor Dave Wildman, as well as Robyn Madrak for their patience, guidance and advice. Also, thanks to everyone in the RF group for making my Fermilab internship enjoyable and productive. Moreover, I want to thank my two mentors Dave Peterson and Elmie Peoples-Evans for always being there to listen. Finally, I thank Dr. James Davenport for his help with this paper.

References

[1] "Neutrinos," http://www-donut.fnal.gov/web_pages/neutrinospg/Neutrinos.html [Accessed: July 29, 2009].

[2] "NuMI/MINOS facts for neighbors," http://www.fnal.gov/pub/about/communication/neutrinos/ [Accessed: July 17, 2009].

[3] "The NOvA Experiment," http://www-nova.fnal.gov/nova_experiment_print.html [Accessed: July 17, 2009].

[4] K. Seiya et al. "Multi-Batch Slip Stacking in the Main Injector at FermiLab," Proceedings of the 22nd Particle Accelerator Conference, June 25th-29th, 2007, Albuquerque, New Mexico, USA.

[5] B.H. Smith, "Radiofrequency system of the Berkeley 88-inch Cyclotron," Nuclear Instruments and Methods, Vol. 18, 1962, p.184-193.

[6] L.C. Maier, Jr. and J.C. Slater, "Field Strength Measurements in Resonant Cavities," Journal of Applies Physics, vol. 23, no. 1, pp. 68-77, January 1952.

[7] J.E. Griffin, A Numerical Example of an RF Accelerating System", in R.A. Carrigan, F.R.Huson, and M. Month, ed., *Physics of High Energy Particle Accelerators (Fermilab Summer School, 1981),* American Institute of Physics, New York, 1982, p. 564-582.

Appendix

Table 1: Q value and first measured higher order modes

Frequency (MHz)	Q-value	Loss (dB)
52.8895	4622	-40.195
148.8175	5168	-41.593
152.1185	6649	-63.015
156.6632	5864	-25.144
211.9923	848	-50.333
220.5799	6821	-57.045
243.9924	377	-55.040
260.0736	354	-57.580
265.3069	2253	-61.620
277.7591	2488	-50.120
308.0431	452	-63.410
313.5562	2845	-38.860
315.8447	3269	-27.172
326.1133	1794	-51.600
339.0806	2603	-45.775
383.9342	747	-52.573
392.9756	3172	-51.730
394.2333	4920	-39.114
396.3793	5318	-18.675
399.4000	5326	-30.229
404.1878	687	-57.819
426.5231	713	-52.202
433.8333	480	-64.317
478.3982	198	-44.925
480.3467	3112	-39.551
485.1953	517	-38.912
515.9766	914	-44.028
521.6352	678	-56.529
529.2849	266	-48.221
544.9068	265	-52.377
551.6047	445	-50.717
559.6693	4680	-27.108
565.1249	1083	-32.037
578.9018	423	-52.736
593.0613	330	-47.227
601.4851	795	-48.728

Table 2: Measurements of Frequency with respect to gap distance

gap distance (in)	gap distance (m)	Frequency -trial 1	Frequency - trial 2	Calculated Frequency (MHz)
1.5	0.0381	44.045	46.579	45.522
2.5	0.0635	51.681	51.433	50.902
3.5	0.0889	53.521	53.378	53.336
4.5	0.1143	54.426	54.345	54.712
5.5	0.1397	54.998	54.932	55.595
6.5	0.1651	55.352	55.334	56.209
7.5	0.1905	55.590	55.580	56.661
8.5	0.2159	55.765	55.747	57.006
9.5	0.2413	55.879	55.878	57.280

Table 3: Frequency at a constant gap distance (3.5") with respect to tuner length

	Center End	Shorted End	Gap End
Tuner length (in)	Frequency (MHz)	Frequency (MHz)	Frequency (MHz)
0.0	53.3437	53.2457	53.2688
0.1	53.3374	53.2478	53.2428
0.2	53.3366	53.2521	53.2389
0.3	53.3348	53.2566	53.2346
0.4	53.3303	53.2586	53.2275
0.5	53.3262	53.2628	53.2194
0.6	53.3214	53.2661	53.216
0.7	53.3182	53.2703	53.2103
0.8	53.3164	53.2724	53.2021
0.9	53.3124	53.2764	53.1979
1.0	53.3021	53.2824	53.19
1.1	53.2934	53.2837	53.1784
1.2	53.2917	53.2885	53.1609
1.3	53.2778	53.2930	53.1384
1.4	53.2739	53.2993	53.1212
1.5	53.2590	53.3016	53.1000
1.6	53.2452	53.3075	53.0575
1.7	53.2321	53.3113	53.0525
1.8	53.2108	N/A	53.0249

Table 5: Record of ALL Higher Order Frequency Modes

52.65743
149.29344
153.63287
256.03394
218.81737
221.61862
250.63153
274.04195
306.81203
310.01315
316.27794
321.21844
337.42565
387.04774
391.44970
393.85077
397.45237
399.99100
428.41776
430.21889
430.81926
470.84428
474.04628
479.44966
482.85178
487.25453
517.61101
520.01251
525.81614
548.63039
554.23390
557.43590
560.83802
563.63978
566.64165

569.64353
594.05879
596.59787
615.80988
633.02064
634.82176
640.82552
642.22639
645.82864
657.63602
659.43150
663.43965
664.64040
668.44278
670.04378
694.05879
709.00563
716.61038
718.21138
719.41213
721.01313
731.21951
758.23640
759.43715
762.83928
763.83990
771.04400
784.45278
790.45654
791.85741
792.65791
807.60475
808.40525
813.00813
815.40963

824.41526
826.01626
828.01751
834.42151
836.62289
871.84490
873.24578
874.64665
880.85053
882.05128
886.25319
896.66041
897.59850
902.20138
908.80550
911.00688
914.00876
915.20951
918.21138
930.61914
933.22076
944.02752
945.62852
951.23202
952.43277
968.24265
969.84365
975.04900
975.84741
982.45153
985.25328
989.79362
990.25641

Table 6: Record of all modes up to 530MHz and their associated calculated frequency and type

Measured frequency	Calculated frequency	Type of mode
52.65743	52.814	Main TEM
149.29344	141.0	$\lambda_g/4$, m=1 Ring
153.63287		
156.03394	158.442	3rd harmonic TEM
218.81737	221.0	$3\lambda_g/4$, m=1 Ring
221.61862		
250.63153	264.07	5th harmonic TEM
274.04195	261.9	$\lambda_g/4$, m=2 Ring
306.81203	312.5	$3\lambda_g/4$, m=2 Ring
310.01315		
316.27794	327.1	$5\lambda_g/4$, m=1 Ring
321.21844		
337.42565	369.698	7th harmonic TEM
387.04774	387.0	$\lambda_g/4$, m=3 Ring
391.44970		
393.85077	394.7	$5\lambda_g/4$, m=2 Ring
397.45237		
399.99100	422.9	$3\lambda_g/4$, m=3 Ring
428.41776	475.326	9th harmonic TEM
430.21889	422.9	$3\lambda_g/4$, m=3 Ring
430.81926	440.7	$7\lambda_g/4$, m=1 Ring
470.84428		
474.04628	486.8	$5\lambda_g/4$, m=3 Ring
479.44966		
482.85178	492.8	$7\lambda_g/4$, m=2 Ring
487.25453		
517.61101	513.3	$\lambda_g/4$, m=4 Ring
520.01251		
525.81614	580.954	11th harmonic TEM